Available online at www.sciencedirect.com
SCIENCE DIRECT®
Journal of Food Engineering 70 (2005) 489–498
JOURNAL OF FOOD ENGINEERING
www.elsevier.com/locate/jfoodeng

Experimental study of hydrodynamics in a flat ohmic cell—impact on fouling by dairy products

M.A. Ayadi [a,*], J.C. Leuliet [a], F. Chopard [b], M. Berthou [c], M. Lebouché [d]

[a] *INRA (Institut National de la Recherche Agronomique), LGPTA (Laboratoire de Génie des Procédés et Technologie Alimentaires), 369, rue Jules Guesde, 59650 Villeneuve D'Ascq Cedex, France*
[b] *ALFA LAVAL VICARB, rue du Rif Tronchard, 38120 Fontanil cornillon, France*
[c] *EDF-R&D, Les Renardières, 77818 Moret sur loing Cedex, France*
[d] *LEMTA, 2, Avenue de la forêt de Haye, 54504 Vandoeuvre-lès-Nancy, France*

Received 12 May 2004; accepted 5 October 2004
Available online 30 November 2004

Abstract

This study highlights the link between hydrodynamics and fouling phenomena in a continuous rectangular ohmic cell. The hydrodynamic study was carried out using flow visualisation techniques and particle image velocimetry (PIV). The distribution of deposits in the ohmic cell was investigated by heating an aqueous solution of β-lactoglobulin-xanthan gum mixture. Experimental results show that the deposit distribution on the electrode surfaces is directly related to the flow structures in the ohmic cell.

Keywords: Ohmic heating; Fouling; Hydrodynamic; Dairy products

1. Introduction

The food industry and in particular the dairy industry, are faced with a severe problem due to equipment fouling during processing. Consequently, several studies have been devoted to heat exchanger fouling by dairy products (Belmar-Beiny, Gotham, Paterson, & Fryer, 1993; Changani, Belmar-Beiny, & Fryer, 1997; Delplace & Leuliet, 1995; Grijspeerdt, Hazarika, & Vucinic, 2003; Lalande, Tissier, & Corrieu, 1985). All these works show the crucial effect of hydrodynamic parameters on fouling phenomena in plate heat exchangers. In spite of the advances in the comprehension of fouling phenomena, the performances of heat exchangers still remain limited by fouling problems. Therefore, the development of alternative technologies for fouling limitation is of interest.

Ohmic heating is one of these new technologies, where the absence of a hot wall should provide a considerable advantage for foodstuff applications, by avoiding the degradation of thermo-sensitive compounds by over-heating and by reducing the fouling of the surfaces during processing. Unfortunately, most studies devoted to this technology have focused on the heat treatment of food fluids with high particle contents, (Benabderrahmane & Pain, 2000; De Alwis, Halden, & Fryer, 1989; Eliot-Godéreaux, 2001; Fryer & De Alwis, 1989; Sudhir, Sastry, & Salengke, 1998; Wadad, Khalaf, Sudhir, & Sastry, 1996) or hydrocolloid solutions (Marcotte, 1999) and did not focus on fouling. Moreover, most of these studies were carried out using tubular geometry with a parallel electric field-flow configuration $\vec{E}\|\vec{V}$ ($\vec{E}$: electric field and $\vec{V}$: velocity field). Ould El Moktar, Peerhossani, and Le Peurian (1993) and El Hajal (1997) studied the combined effect

* Corresponding author. Tel.: +33 3 20 43 54 40; fax: +33 3 20 43 54 26.
E-mail addresses: ayadi-mohamed.ali@lille.inra.fr, ayadimedali@yahoo.fr (M.A. Ayadi).

0260-8774/$ - see front matter © 2004 Elsevier Ltd. All rights reserved.
doi:10.1016/j.jfoodeng.2004.10.004

of hydrodynamic, thermal and electrical phenomena when heating a homogenous non-fouling fluid by a rectangular ohmic channel with a perpendicular electric field-flow configuration ($\vec{E} \perp \vec{V}$). Few scientific studies have been devoted to the heat treatment of fouling food fluids by a rectangular ohmic channel (Ayadi, Bouvier, Chopard, Berthou, & Leuliet, 2003; Ayadi, Chopard, Berthou, & Leuliet, 2004). However, during the heat treatment of fouling food flows by ohmic technology, in addition to the links between the physical phenomena already mentioned by Ould El Moktar et al. (1993) and El Hajal (1997), secondary links between deposit layers and these phenomena appear as soon as the electrodes are fouled. In continuous ohmic heating, thermal behaviour depends on the quantity of energy received by the fluid during its passage through the cell. This quantity of energy depends on the electric field applied and the residence time distribution in the cell expressed by velocity fields. The fluid circulating at a lower than average velocity remains in the electric field longer and receives more energy than the fluid circulating at a velocity higher or equal to the average. This excess energy results in local overheating zones which become more subject to fouling. The presence of a non-uniform flow in a continuous ohmic cell (presence of re-circulation and acceleration zones) is bound to affect its thermal and electric behaviour and thus the intensity and distribution of fouling in it.

The objective of this paper is therefore to identify and study experimentally the impact of hydrodynamic behaviour on the intensity and distribution of fouling deposits, if any exist, in a rectangular ohmic channel with a perpendicular electric field-flow configuration. The hydrodynamic study was carried out with a Newtonian model fluid under isothermal conditions, using a flow visualisation technique (coloured tracer) and the velocity fields were measured using particle image velocimetry (PIV). The distribution of deposits in the ohmic cell was investigated by heating an aqueous solution of a β-lactoglobulin-xanthan gum mixture.

2. Materials and methods

2.1. The experimental cell

The experimental cell, shown in Fig. 1, takes the form of a rectangular channel ($240 \times 75 \times 15$ mm thick). It is composed of a spacer that houses the inlet–outlet devices and two electrodes making up the lateral surfaces. In this work, the influence of two different inlet–outlet orifice geometries on the hydrodynamic and fouling behaviour in the ohmic cell has been investigated. The geometry termed "initial" is composed of two elliptical opening with conical channels (Fig. 1(a)). The geometry

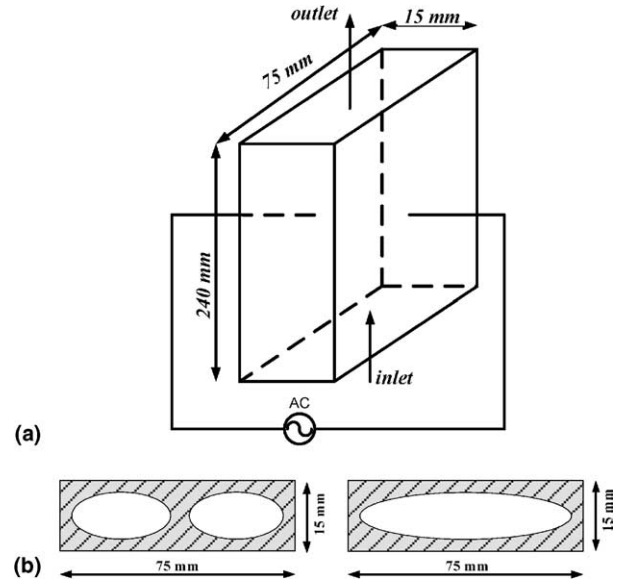

Fig. 1. Geometry of the flat ohmic cell and the studied input–output orifices: (a) initial geometry; (b) modified geometry.

termed "modified" is composed of a single elliptical opening with conical channel (Fig. 1(b)).

2.2. Hydrodynamic study

Flow visualisation tests and velocity field measurements were performed to study the hydrodynamic behaviour in the ohmic cell. The experimental set-up used for the visualisation tests consists of a feed tank, a volumetric pump, an electromagnetic flow meter, an assembly of three transparent cells, a coloured tracer injection system, a static mixer to avoid any risk of poor mixture heterogeneity, a digital camera and a PC for video image acquisition.

Experiments were carried out, in isothermal conditions (20 ± 1 °C), with a sucrose solution at 55% (w/w) whose concentration was selected to obtain a Reynolds number of 65 for a flow of 300 l/h. 5 g of fluorescein powder was added to 100 ml of circulating fluid to act as a coloured tracer.

The coloured tracer was injected just before the cell inlet and its distribution was recorded in the form of video sequences through the transparent surface. This method allowed a qualitative characterisation of the flow. Image processing was performed on the video sequences acquired and included the following key steps:

(i) Sampling of the video image sequences at a frequency of 30 images per second (Video Editor 5.02).
(ii) Coloured tracer passage time, is normalised and reduced by the average residence time ($\tau = \frac{V}{Q}$), with V being the volume of the cell (m^3) and Q the circulation flow (m^3/s).
(iii) Visualisation of the coloured tracer head progression as a function of reduced time: $t^* = \frac{t}{\tau}$.

Velocity fields in the ohmic cell were measured using the particle image velocimetry (PIV) technique. A sketch of the experimental set-up is shown in Fig. 2. A light source including a crystal harmonic generator to produce the double-frequency green light (Nd : YAG; Continum; ML PIV) was added to the experimental set-up used for flow visualisation. A cylindrical lens transformed the light ray into a 0.25 mm thick laser plane. A high resolution CCD camera (Kodak Mega plus ES.1.0) was placed perpendicular to the illuminated plane, permitting the recording of two successive images of the flow in this plane. Two mountings (Dantec Measurements) were used for accurate laser plane and CCD camera displacement. A flowmap type synchroniser (Dantec Measurement Technology, Denmark) ensured the synchronisation of the illumination frequency and recording images.

The fluid chosen was the same as that used to visualise the flow. It should also be noted that reflective particles were added to the fluid beforehand (Dantec Measurement Technology; France, diameter 15 μm and density = 1.4 g cm^{-3}).

Each pair of images of $1008 \times 1016\,px^2$ recorded by the CCD camera was divided into small interrogation areas $32 \times 32\,px^2$ with a 25% overlap. The averages and standard deviations were calculated using 625 instantaneous measurements.

2.3. Heating of a model fouling fluid inside the ohmic cell

The experimental set-up used during thermal treatment (heating) of the model fouling fluid is shown in Fig. 3. This set-up comprises three distinct zones: a preheating zone composed of a classical plate heat exchanger, a heating zone composed of an assembly of five ohmic cells (study zone) and a cooling zone composed of a tube heat exchanger.

The flow was measured by an electromagnetic flow meter (Khrone, type:IFM 10,807 K). The temperatures were measured by platinum resistance probes (type Pt 100) placed at the inlet and outlet of each zone. A differential pressure sensor (Schlumberger, type:D) was used to monitor pressure drop variations in the five ohmic cells. Electric power was applied using a 15 kW generator and a three-phase system. Voltage (voltmeter 0–250 V, Sineax U504, Chauvin Arnoux) and current intensity (Ammeter 0–200 A, type AC22, Camille Bauer) were measured in the third phase.

During all the fouling experiments the flow was kept constant at 300 l/h (Re_g = 65) and the inlet and outlet temperatures in the cells were respectively 75 °C and 100 °C (choice relating to the protein denaturation temperature of approximately 80 °C). Several test durations were set to monitor the onset and the progression of any fouling. Operating conditions are summarised in Table 1 (tests 3–4 and 7–8 were performed to test reproducibility).

Given the advantages that a model fluid could provide (reproducibility, control over physical properties, etc.), an aqueous solution of a β-lactoglobulin-xanthan gum mixture (1% w/w of protein and 0.2% w/w of xanthan gum) was chosen as a model fouling fluid. β-lactoglobulin is to a great extent responsible for the fouling caused by dairy products (Lalande et al., 1985). Xanthan gum was used to adjust the fluid's viscosity.

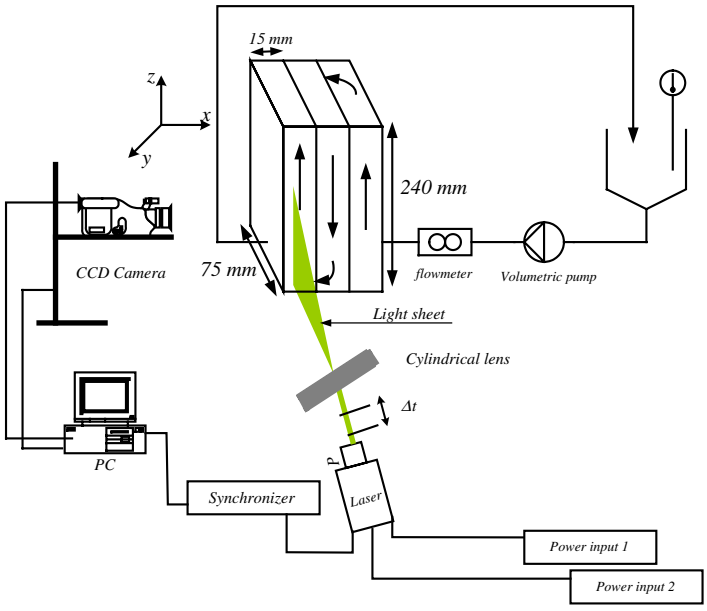

Fig. 2. PIV measurement: pilot plant.

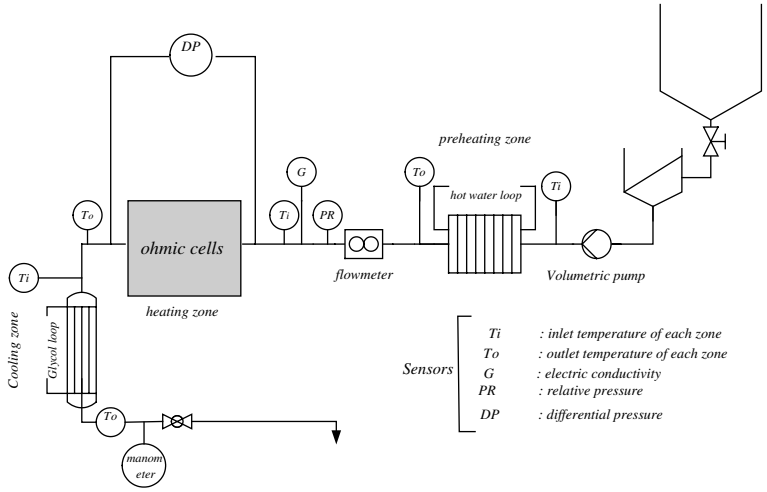

Fig. 3. Heat treatment of the fouling model fluid: experimental device.

Table 1
Fouling tests: operating conditions

Test no.	Duration (h)	Inlet–outlet orifice geometry
1	1	Initial
2	2	Initial
3 and 4	3	Initial
5	1	Modified
6	2	Modified
7 and 8	3	Modified

The model fluid was prepared with great care to ensure that its physical properties remained constant for all the tests:

- pH from 7 to 7.1.
- Shear thinning behaviour: described by Ostwald's law: $n = 0.0023\theta + 0.234$ and $k = 6.78\theta^{-0.663}$ with θ from 20–80 °C and $\dot{\gamma}$ from 0.4 to 700 s^{-1}.
- Electric conductivity progressing linearly with temperature and described by the following relation: $\sigma = 1.35 + 0.0383(\theta - 20)$ for temperatures varying from 0 to 100 °C.

All the other physical properties (density, specific heat, thermal conductivity) were very close to those of water.

After each fouling test, the system was dismantled and following steps were carried out: (i) the electrodes and spacers were dried for 6 h at 100 °C; (ii) the dried deposit mass per cell was measured; and (iii) photographs were taken of the fouled electrodes.

Once these steps had been completed, the distribution of the deposit on the two electrodes was determined, by dividing the electrode surfaces into twelve parts (6 mm × 2.5 mm). Each part was dampened with 3 ml of distilled water. The dampened deposit was scraped, dried and then weighed in precision scales (Precisa Instrument; 202A; ±0.1 mg; Switzerland). This method allowed the determination of deposit distribution on the electrode surfaces.

The precision of this method was verified by systematically comparing the deposit mass on the entire surface of the electrode and the total masses of the deposits on the twelve parts. The difference never exceeded 15%.

3. Results and discussion

3.1. Hydrodynamic study

3.1.1. Cell with initial geometry orifice

Fig. 4 shows a succession of photographs illustrating the passage of the coloured tracer in the ohmic cell equipped with the initial geometry orifice. This figure clearly shows that following the passage of the fluid via the inlet orifice, the flow profile becomes deformed into two distinct parabolic profiles. This deformation can largely be explained by the geometry of the inlet orifice, particularly the separation between the two opening channels ($35 < y < 45$ mm). The conical bore and the separation of these two opening holes favour an accelerated flow at the extension of the holes ($10 < y < 30$ mm and $50 < y < 65$) and lead to a slower flow in the central zone ($35 < y < 45$ mm). The progression of the tracer in the cell shows that the global structure of the flow is strongly influenced by the disturbance due to the passage through the inlet orifice. By moving from the inlet to the outlet of the cell, we were able to observe that the flow structure favours the appearance of secondary flows at the inlet zone. The progression of the tracer towards the centre of the cell showed that the space between the two parabolic profiles narrows as the tracer advances. Conversely, the two non-mixing zones close to the side walls were always present. Towards the outlet

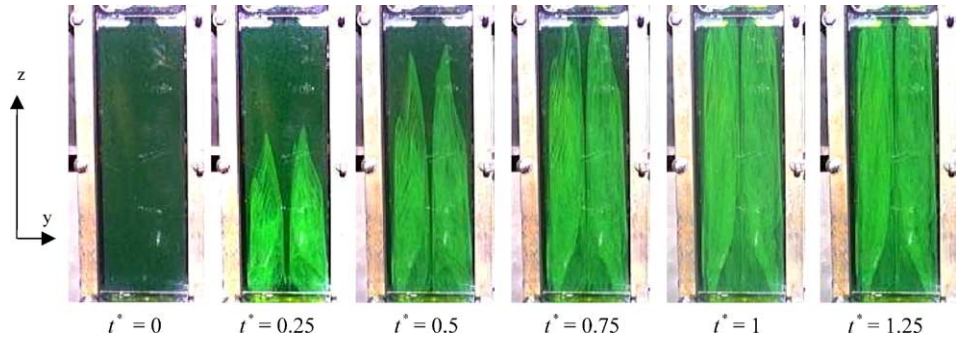

Fig. 4. Flow visualisation at $Re = 65$ using the coloured tracer: cell equipped with initial geometry orifice.

of the cell, even though the flow tended to a more homogenous profile, the deformation of the flow pattern due to the disturbances at the inlet still remained visible.

These visualisation tests are important since they permit the qualitative identification of flow patterns in the cell and highlight the influence of the orifice's geometry on the flow profile in the ohmic cell. However, it was still necessary to quantify and verify whether the behaviour observed was valid for the entire thickness of the cell. To achieve this, measurements of the velocity fields were carried out in the central plane of the ohmic cell ($x = 7.5$ mm).

The instantaneous velocity vector maps and the flow streamlines in the inlet zone of the cell equipped with an initial orifice geometry are presented in Fig. 5. This figure shows the existence of a preferential passage in the continuity of the opening channels and a low speed zone at the centre of the inlet zone. This result shows that the flow patterns observed during visualisation using the coloured tracer are the same along the entire thickness of the cell. In addition to the heterogeneity of the velocity vectors at the cell inlet, Fig. 5(b) shows a progressive deviation of the flow lines towards the side walls. This deviation is due to the conical shape of the inlet orifice. The presence of an undulation at the edge of the walls ($55 < z < 65$ mm) was seen to change progressively into a succession of vortex structures ($15 < y < 55$ mm and $35 < z < 65$ mm). The flows initially directed upstream change direction following contact with the side wall, returning downstream and give rise to vortex-like structures.

The presence of these secondary flows in the inlet zone certainly has an influence on the establishment of the flow in the ohmic cell. In order to evaluate this influence Fig. 6 shows velocity profiles at different level of the cell high ($z = 30$ mm, $z = 90$ mm, $z = 150$ mm and $z = 210$ mm). This figure shows that the velocity profile at the inlet is considerably disturbed and diverges from a parabolic profile. This profile has a hollow in the centre of the passage section ($10 < y < 60$ mm) and two peaks in the extension of the channels ($3 < y < 10$ mm and $60 < y < 67$ mm). The two velocity profiles at the centre and at the outlet of the cell show that the flow tends towards the establishment of a Newtonian type parabolic profile, since we observed a progressive flattening of the central hollow and the disappearance of the two peaks observed at the inlet of the cell. Despite this improvement, the velocity profiles at the cell's outlet was still slightly deformed and the flow not completely established.

The geometry of the inlet orifice of the ohmic cell was modified in the light of the results of this first

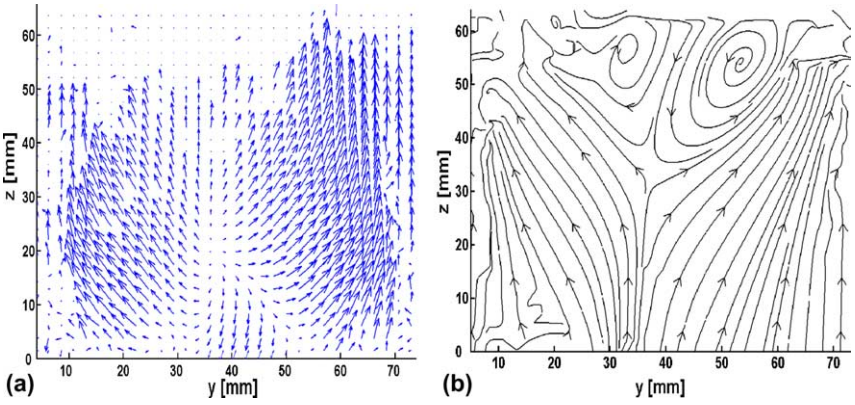

Fig. 5. Flow at the central plan ($x = 7.5$ mm) in the entrance zone of the cell equipped with an initial geometry opening: (a) instantaneous velocity vector map; (b) instantaneous streamlines.

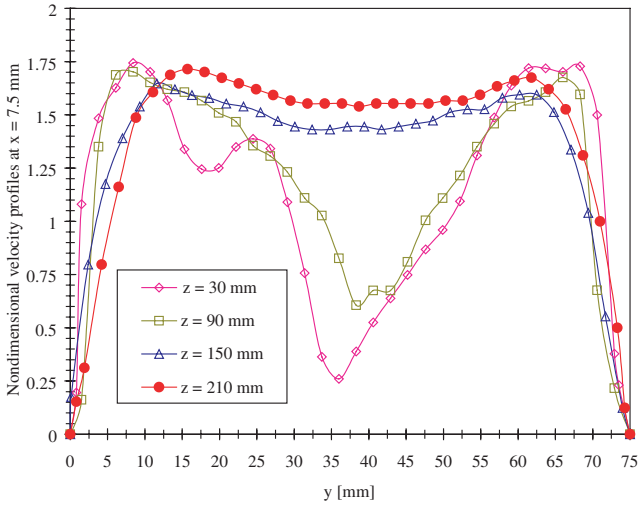

Fig. 6. Velocity profiles at the central plane ($x = 7.5$ mm) in the ohmic cell equipped with an initial geometry opening.

hydrodynamic study. The study of the flow in the cell equipped with the new geometry was carried out under the same conditions as those performed for the cell equipped with the initial geometry.

3.1.2. Cell with modified geometry orifice

Fig. 7 shows a sequence of photographs illustrating the passage of the coloured tracer in the ohmic cell equipped with an inlet orifice whose geometry had been modified. Observation of these photographs shows that the inlet orifice with modified geometry appears to improve the uniformity of the flow in the cell. The simple geometry of the orifice allows the fluid to pass without over-modifying its flow profile. We noted the absence of the deceleration zone in the centre of the cell ($10 < y < 30$ mm and $50 < y < 65$) and the two acceleration zones seen previously. In spite of this improvement, we nonetheless noticed a slight deformation of the advancing profile of the coloured tracer. This deformation was mainly due to the sudden passage from one cell to another (succession of two orifices: outlet of the first cell followed by the inlet of the second).

The instantaneous velocity field and the streamlines at the cell inlet equipped with an orifice of different geometries are presented in Fig. 8. This figure confirms the improvement of the flow already observed during visualisation. Most of the velocity vectors take the direction of the flow. It should be noted that the preferential flow zones and vortex structures have disappeared.

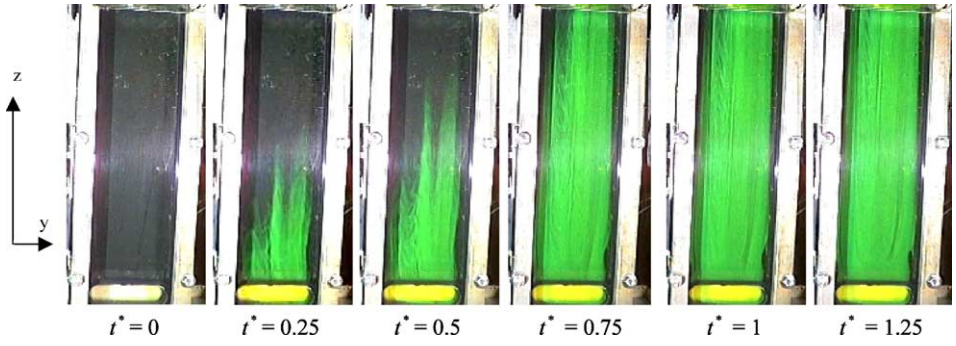

Fig. 7. Flow visualisation at $Re = 65$ using the coloured tracer: cell equipped with modified geometry orifice.

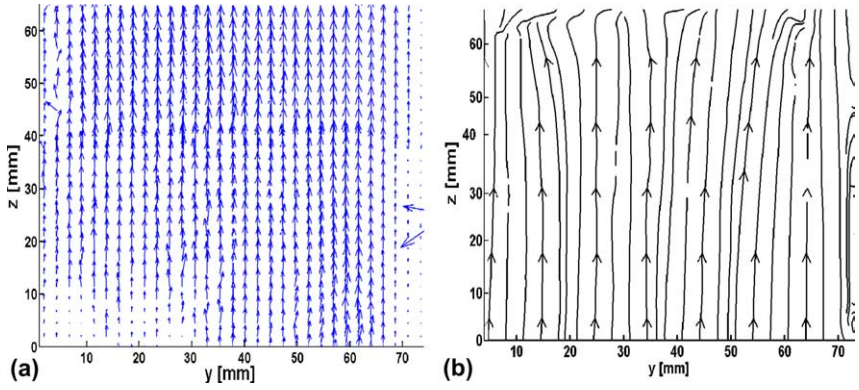

Fig. 8. Flow at the central plan ($x = 7.5$ mm) in the entrance zone of the cell equipped with a modified geometry opening: (a) instantaneous velocity vectors map; (b) instantaneous streamlines.

However, a slight disturbance of the flow at the cell inlet can be observed (Fig. 8(a) $0 < z < 20$ mm).

Fig. 9 shows the velocity profiles in the cell equipped with orifices whose geometry had been modified. This figure shows that the velocity profiles at the cell inlet is less disturbed than in the case of the initial geometry. Observation of the velocity profiles in the centre and outlet of the cell shows a faster flow establishment than that in the cell equipped with an orifice with the initial geometry. We noticed a slight disturbance of the velocity profiles in the centre of the cell and an almost established flow in the cell outlet zone.

The length of flow establishment (Z_e) greatly depends on the shape and geometry of the connection between the two channels and the Reynolds number (Comolet, 1982). In practice it is chosen as the distance at end of which the velocity profile draws close to 1% of the parabolic profile. Z_e could be estimated by the following formula:

$$\frac{Z_e}{D} = A \cdot Re \tag{1}$$

D is the diameter of the conduit and Re is the Reynolds number. Several values for coefficient A have been proposed in the literature. Mc Thomas (1967) proposed the value of 0.026 in a laminar regime for a Newtonian fluid in a tubular channel. In other works the same author modified this coefficient, placing it between 0.03 and 0.035. Comolet (1982) proposed a value for coefficient A for each interval of the Reynolds number. For low Reynolds number values, he proposed the value of 0.06. This difference in value assigned to coefficient A, shows that the determination of the length of flow establishment in a channel remains specific to each case and geometry studied. In the case of this study, by taking into account the value proposed by Comolet (1982), the length of establishment equals 27.5 mm. This means that theatrically, at $z = 30$ mm, the velocity profile draws close to 1% of the parabolic profile. Fig. 6 shows that in the case of the ohmic cell equipped with orifices having the initial geometry, the flow is not perfectly parabolic even after a length of 210 mm (profile at the outlet of the cell). However, Fig. 9 shows that in the case of the cell equipped with an orifice whose geometry has been modified, the velocity vector profile is very close to that of a parabolic profile from $z = 150$ mm (profiles in the centre and outlet of the cell).

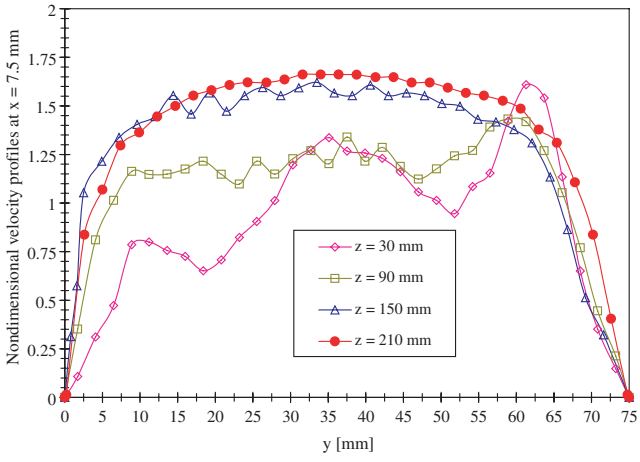

Fig. 9. Velocity profiles at the central plane ($x = 7.5$ mm) in the ohmic cell equipped with a modified geometry opening.

3.2. Thermal treatment of the model fouling fluid

3.2.1. Reproducibility of fouling tests

The reproducibility of fouling tests was estimated by measuring the mass of deposits on the electrodes, the progression of pressure drop as a function of time and the progression of electric variables (current, voltage). The comparison of these different tests based on these criteria showed itself to be quite positive (±5%).

3.2.2. Progression of deposit masses

Fig. 10 illustrates the deposit masses as a function of time, for all the tests performed and the two geometries tested. These results clearly show that fouling was relatively low after 2 h of operation and became much heavier for an operating time of 3 h. This leads us to suppose that, as in plate and joint heat exchangers (Lalande et al., 1985) and tubular heat exchangers (Fryer,

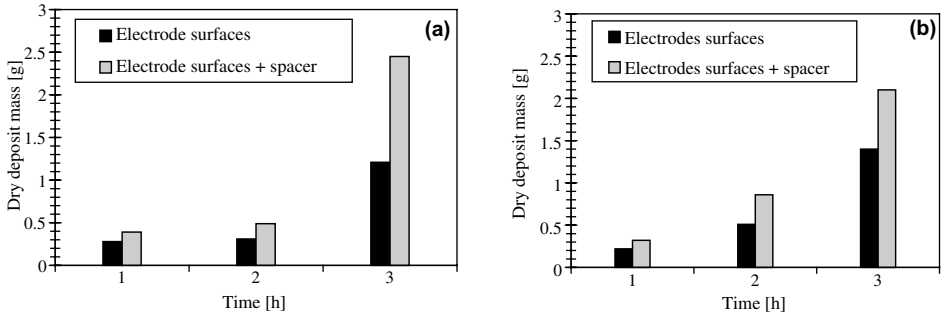

Fig. 10. Dry deposit mass after 1, 2 and 3 h-fouling experiments: (a) cell equipped with initial geometry orifice; (b) cell equipped with modified geometry orifice.

1989), a fouling induction period exists before it reaches very high levels.

For the two 3 h tests, it would appear that the deposit mass is lower in the cells whose geometries were not modified. Although this is true, very large quantities of deposit could be seen in the inlet–outlet orifices of these non-modified cells (in the spacer). This means that for the entire cell, the total deposit mass (electrode surfaces + spacer) is greater for the cells with the initial geometry. These very substantial deposits in the inlet–outlet orifices can quickly result in the installation becoming clogged.

3.3. Fouling–hydrodynamic links

Fig. 11 is a photograph of two electrodes fouled after 1 and 2 h-fouling runs (test 5 and 6). This figure clearly shows that the inlet zone of the cell is subject to a far more rapid deposit than anywhere else. This phenomenon cannot easily be linked to temperature since the fluid temperature at the outlet of the cell is higher than at its inlet ($\Delta t = 8.5\,^{\circ}C$). On the contrary, by referring to the hydrodynamic study carried out previously, it could be seen that fouling starts at the point where the velocities are least uniform.

Fig. 12 presents photographs of the electrode surfaces after 3 h-fouling runs (test 4 and 7). This figure shows that appearance and distribution of the deposits on the electrodes is very similar to the distribution of the coloured tracer during the visualisation tests. Indeed, in Fig. 12(a) (initial geometry) three distinct zones can be seen: (i) a heavily fouled zone at the cell inlet with a spiral deposit profile ($0 < z < 70$ mm), (ii) a slightly fouled zone with a parabolic deposit profile. This zone corresponds to the extension of the channels of the passage where the maximum velocities were recorded; and (iii)

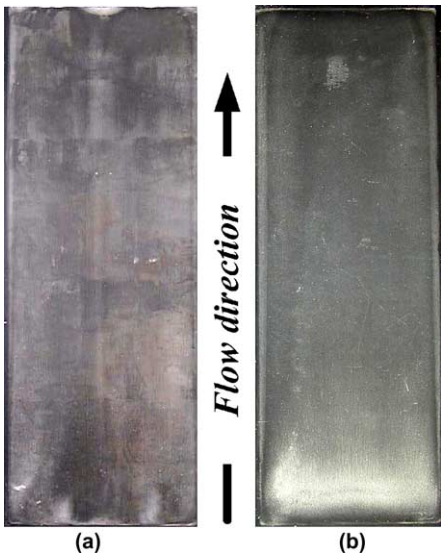

Fig. 11. Electrode photo: (a) after 1 h-fouling run; (b) after 2 h-fouling run.

an averagely fouled zone corresponding to the extension of the mechanical separation situated next to the side walls. It should be recalled that this zone corresponds to the deceleration zones identified during the hydrodynamic study. The same conclusions can be drawn from Fig. 12(b): the fouling is more homogenous in the cell equipped with an orifice with modified geometry in spite of a heavily fouled zone at the cell inlet. It therefore seems that the presence and intensity of the deposit in the cells is directly linked to the uniformity and non-uniformity of the velocities.

To appreciate the quantity of material deposited locally on each of the cells, deposit mass measurements are shown in Fig. 13. The two 3 h-fouling tests are represented for both the initial geometry and the modified

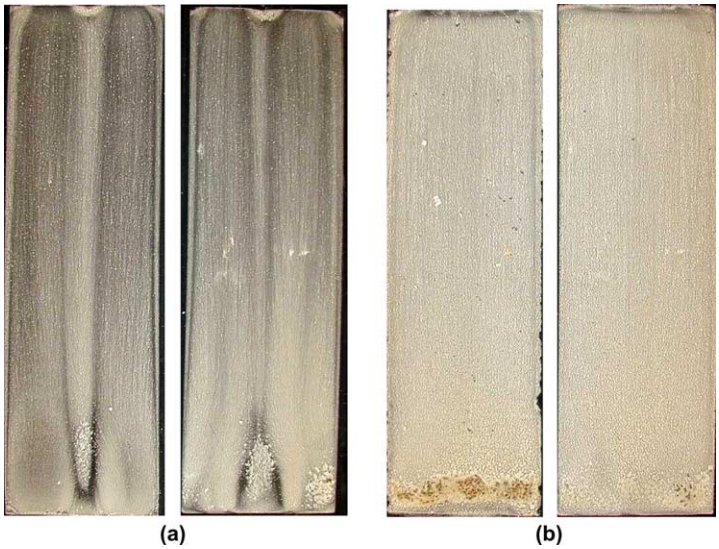

Fig. 12. Electrode photo after 3 h-fouling test: (a) cell equipped with initial geometry orifice; (b) cell equipped with modified geometry orifice.

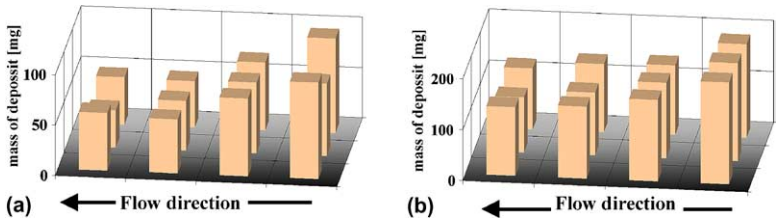

Fig. 13. Deposit mass distribution on the electrode surfaces after 3 h-fouling test: (a) cell equipped with initial geometry orifice; (b) cell equipped with modified geometry orifice.

geometry. Using a far more quantitative approach than previously, this figure once again shows that the mass distribution is far more uniform for the modified geometry (test 7) than for the initial geometry (test 4). Moreover, there does not appear to be any correlation between the quantity of deposit and the temperature in the centre of the ohmic cell; the deposit is always heavier in the inlet zone where the temperature is lowest. It should be noted that this zone corresponds to the re-circulation zone identified during the hydrodynamic study.

This leads us to confirm the previous conclusions: the onset, presence and intensity of the deposit in the ohmic cell are directly linked to the uniformity or non-uniformity of velocities.

4. Conclusions

Hydrodynamic behaviour in a flat ohmic cell was studied using flow visualisation and PIV techniques. This hydrodynamic study with a Newtonian fluid in an isothermal situation allowed firstly, a better understanding to be acquired of the velocity vector distribution in the ohmic cell. Secondly it permitted the flow structure to be improved simply by changing the geometry of the cell's input–output orifices. Finally the estimation became possible of the inlet length in the ohmic cell.

Heat treatment of a model fouling fluid shows that the quantity of deposit is greater in the zone where the temperature is lowest (entrance zone) and the velocity is non-uniform. These results clearly show that in continuous ohmic heating, even the slightest hydrodynamic disturbance (re-circulation, poor filling, singularity, etc.) results in a thermal and electric disturbance and there by creates zones, which are subject to fouling. Future works will be devoted to the investigation of the temperature gradients between electrode surfaces and the bulk under fouling conditions.

Acknowledgements

The authors would like to express their thanks to Michel Gradeck and Luc Fillaudeau for their contribution to the PIV measurements.

The authors gratefully acknowledge the financial support from Alfa Laval Vicarb and Electricité de France.

References

Ayadi, M. A., Bouvier, L., Chopard, F., Berthou, M., & Leuliet, J. C. (2003). Heat treatment improvement of dairy products via ohmic heating process: thermal and hydrodynamic effect on fouling. *Heat Exchanger Fouling and Cleaning—Fundamentals and Applications*. Engineering Conference International (ECI), New Mexico, Santa Fe, USA.

Ayadi, M. A., Chopard, F., Berthou, M., & Leuliet, J.-C. (2004). Ohmic heating unit performance under whey proteins fouling. In *Proceeding of the ninth international conference engineering and food (ICEF 9)*, Montpellier, France.

Belmar-Beiny, M. T., Gotham, S. M., Paterson, W. R., & Fryer, P. J. (1993). The effect of Reynolds number and fluid temperature in whey protein fouling. *Journal of Food Engineering, 19*, 119–139.

Benabderrahmane, Y., & Pain, J. P. (2000). Thermal behaviour of a solid/liquid mixture in an ohmic heating sterilizer—slip phase model. *Chemical Engineering Science, 55*, 1371–1384.

Changani, S. D., Belmar-Beiny, M. T., & Fryer, P. J. (1997). Engineering and chemical factors associated with fouling and cleaning in milk processing. *Experimental Thermal and Fluid Science, 14*, 392–406.

Comolet, R. (1982). *Mécanique expérimentale des fluides* (3rd ed.). Paris: Masson, pp. 92–100.

De Alwis, A. A. P., Halden, K., & Fryer, P. J. (1989). Shape and conductivity effects in the ohmic heating of foods. *Chemical Engineering Research and Design, 67*, 159–168.

Delplace, F., & Leuliet, J. C. (1995). Modeling fouling of a plate heat exchanger with different flow arrangements by whey protein solutions. *Trans Ichem, 73*, 112–120.

El Hajal, J. (1997). *Étude expérimentale et numérique de la convection mixte dans un écoulement de poiseuille en présence d'une dissipation volumique d'énergie par conduction électrique directe*. Ph.D. thesis, Nantes University, France.

Eliot-Godéreaux, S., Zuber, F., & Goullieux, A. (2001). Processing and stabilisation of cauliflower by ohmic heating technology. *Innovative Food Science and Emerging Technologies, 2*, 279–287.

Fryer, P. G. (1989). The use of fouling models in the design of food process plant. *Journal of the Society of Dairy Technology, 42*, 23–29.

Fryer, P. J., & De Alwis, A. (1989). Validation of the APV ohmic heating process. *Chemistry and Industry, 16*, 630–634.

Grijspeerdt, K., Hazarika, B., & Vucinic, D. (2003). Application of computational fluid dynamics to model the hydrodynamics of plate heat exchangers for milk processing. *Journal of Food Engineering, 57*, 237–242.

Lalande, M., Tissier, J. P., & Corrieu, G. (1985). Fouling of heat transfer surfaces related to β-lactoglobulin denaturation during heat processing of milk. *Biotechnology Progress, 1*, 131–139.

Marcotte, M. (1999). *Ohmic heating of viscous liquid food*. Ph.D. thesis, Department of Food Science and Agricultural Chemistry, University Mc Gill, Canada.

Mc Thomas, S. T. (1967). Hydrodynamic entrance lengths for duct of arbitrary cross section. *Journal of Basic Engineering*, 847–850.

Ould El Moktar, A., Peerhossani, H., & Le Peurian, P. (1993). Ohmic heating of complex fluids. *International Journal of Heat and Mass Transfer, 36*(12), 3143–3152.

Sudhir, K., Sastry, S. K., & Salengke, S. (1998). Ohmic heating of solid–liquid mixtures: a comparison of mathematical models under worst-case heating conditions. *Journal of Food Process Engineering, 21*, 441–458.

Wadad, G., Khalaf Sudhir, K., & Sastry, S. K. (1996). Effect of fluid viscosity on the ohmic heating rate of solid–liquid mixtures. *Journal of Food Engineering, 27*, 145–158.